Cichocki, F., et al. Electric propulsion subsystem optimization for "Ion Beam Shepherd" missions. In: *Journal of propulsion and power, 33(2), March 2017, Pp. 370-378*

DOI: https://doi.org/10.2514/1.B36105

<

# Electric Propulsion Subsystem Optimization for "Ion Beam Shepherd" Missions

F. Cichocki[1], M. Merino[2] and E. Ahedo[3]
*Universidad Carlos III de Madrid, Leganés, Spain*

M. Smirnova[4], A.Mingo[5]
*TransMit GmbH, Gießen, Germany*

M.Dobkevicius[6]
*University of Southampton, Southampton, UK*

**The ion beam shepherd is an innovative contactless technique for space debris removal, in which an impulse transfer thruster pushes the debris object through the action of a plasma plume and an impulse compensation thruster maintains formation flying. The optimal operational point of both thrusters strongly depends on their characteristics and on the physics of the plasma plume expansion into vacuum. With the use of dedicated thruster performance models, complemented with simplified plume expansion and plasma-debris interaction models, a system-level optimization study of the impulse transfer thruster alone and of the overall electric propulsion subsystem is presented for an ion beam shepherd mission example. An optimum design point is found for minimum overall power consumption in both cases.**

---

[1] PhD student, Equipo de Propulsión Espacial y Plasmas, filippo.cichocki@uc3m.es
[2] Assistant professor, Equipo de Propulsión Espacial y Plasmas, mario.merino@uc3m.es
[3] Professor, Equipo de Propulsión Espacial y Plasmas, eduardo.ahedo@uc3m.es
[4] Head of the IQM, Maria.Smirnova@transmit.de
[5] Project Manager, IQM, aloha.mingo@transmit.de
[6] PhD Student, md4g09@soton.ac.uk

**Nomenclature**

$\alpha_0$ = Initial divergence angle of the 95% ion current streamtube

$\alpha_F$ = Equivalent conical divergence angle of the 95% ion current streamtube at 7 m distance

$\eta_B$ = Momentum transfer efficiency of the beam

$\eta_m$ = Mass utilization efficiency

$\eta_T$ = Total thrust efficiency

$\phi$ = Electric potential with respect to the S/C ground

$\rho$ = Specific mass per unit of power

$\Delta\phi$ = Electric potential drop or growth (assumed positive)

$\Delta t_{IBS}$ = Duration of the IBS shepherding phase

$\Delta V$ = Electric propulsion delta-V

$d$ = Distance between the thruster and the geometrical centre of the target debris

$d_0$ = Axial extension of the near region of the plasma plume

$e$ = Electron charge

$f_{light}$ = Fraction of the orbital period in daylight conditions

$F$ = Thrust force

$h$ = Self-similarity function in the self-similar plume model

$I$ = Electric current

$I_{sp}$ = Specific impulse

$n$ = Plasma plume number density

$M_0$ = Plasma plume initial ion Mach number

$m$ = Mass

$\dot{m}$ = Mass flow rate of the electric thruster

$q$ = Electric charge

$(r, z)$ = Radial and axial coordinates in the plasma plume reference frame

$\tilde{r}$, $\tilde{z}$ = Radial and axial coordinates, normalized with $R_0$

$P$ = Input thruster power

$R_0$ = Initial radius of the 95% ion current streamtube

$R_F$ = Final radius of the 95% ion current streamtube at 7 m distance

$R_{thr}$ = Thruster radius

$R_{TG}$ = Radius of the equivalent sphere of the target debris

$T_e$ = Electron temperature

$u_z$ = Plasma plume axial velocity

$u_r$ = Plasma plume radial velocity

**Subscripts and superscripts**

$0$ = At the initial plane or at the origin of the far region plume

$F$ = At a distance of 7 m from the initial plane of the far region plume

$acc$ = Acceleration grid

$B$ = Plasma beam

$chamber$ = Inside the discharge chamber

$eq$ = Equivalent from a subsystem point of view

$e$ = Electrons

$i$ = Ions

$IBS$ = Ion beam shepherd spacecraft

$ICT$ = Impulse compensation thruster

$ITT$ = Impulse transfer thruster

$neut$ = Plume neutralization process

$TG$ = Target space debris object

$*$ = To be optimized

$PPU$ = Power processing units

$prop$ = Propellant

$pwr$ = Dedicated power generation subsystem

$RF$ = Radio-frequency discharge

$screen$ = Screen grid

## I. Introduction

The interest and concern of the scientific community in the space debris problem has been constantly growing in the last decade. The increasing number of space debris objects that populate certain types of orbits (especially the Sun synchronous low Earth orbits and the geostationary orbits) can potentially threaten their exploitation in a relatively close future [1–3] and, therefore, demands an international effort in two major fields: mitigation strategies and active debris removal/relocation.

First of all, regarding mitigation, it is necessary to define common and international disposal strategies at the end of life of both commercial and scientific satellites. This represents an extra cost to be added to the mission budget (e.g. extra propellant to transfer the satellite from its operative orbit to a disposal orbit) and it ought to be common to all space competitors in the international scene.

Secondly, efforts have to be put into investigating and demonstrating the technical feasibility of active debris removal (ADR) techniques, which are necessary to effectively stop the growth of the space debris population. In fact, according to a recent study [2], even if all new launches respected the most recent legislation on post-mission disposal strategies (final S/C disposal to a 25-year decay orbit), at least 5 debris objects per year would need to be actively de-orbited in order to prevent the debris number from growing, due to collisions and explosions in the already existing population.

Among many proposed techniques for ADR, the ion beam shepherd (IBS) [4–6] is being considered as a potential candidate by the European Commission, which is currently financing the LEOSWEEP project ("Improving Low Earth Orbit Security With Enhanced Electric Propulsion" [7]), its major goals being the study of the technical feasibility of the IBS technique and the advance in the design of the related technologies.

The IBS concept is briefly described hereafter. Referring to Fig. 1, an ion beam shepherd S/C makes use of an onboard electric thruster to direct a plasma beam against a target debris. This thruster is called impulse transfer thruster (ITT) because the impact of the hypersonic ions of its plume produces a net force on the target, which can be de-orbited or repositioned "contactlessly" and efficiently to a disposal orbit.

However, because of the thruster plume divergence [8, 9], the operating distances are limited to

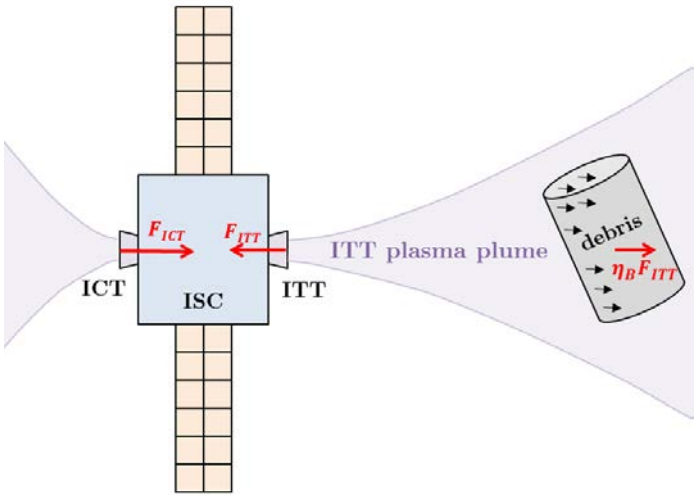


**Fig. 1 Schematic of the ion beam shepherd concept**

a few times the debris size (with the current plasma propulsion technologies). The effective force transferred to the debris is thus only a fraction of the total ITT thrust, $F_{ITT}$, as shown in Eq. 1, with $\eta_B$ representing the momentum transfer efficiency of the beam:

$$F_{TG} = \eta_B F_{ITT}. \tag{1}$$

In order to maintain formation flying, the ITT has to be compensated by an impulse compensation thruster (ICT), which is located on the opposite side of the IBS. More precisely, formation flying demands that the accelerations on both the IBS and the space debris be equal, meaning that the ICT thrust, $F_{ICT}$, is generally higher than that of the ITT [10], as dictated by:

$$F_{ICT} = \left(1 + \eta_B \frac{m_{IBS}}{m_{TG}}\right) F_{ITT} > F_{ITT}, \tag{2}$$

where $m_{IBS}$ and $m_{TG}$ are respectively the IBS and target debris masses.

At system level, it is extremely important to identify the operational points of both thrusters (e.g. the operating voltage and the mass flow rate) that yield the lowest possible system mass, while complying with a vast set of constraints, ranging from overall power availability to size and cost of the required components. Such optimal points strongly depend on the distance between the IBS and the debris object and on the mission specifications. This paper's main goal is to propose an approach for the optimization of the ITT alone and of the overall electric propulsion subsystem (EPS), considering a realistic IBS mission scenario. A preliminary version of this work has already

been presented at the $34^{th}$ International Electric Propulsion Conference [11].

Before proceeding with the description of the optimization study, the mission specifications and the IBS power constraints and assumptions are described in Sec. II. The ITT and ICT performance models are introduced in Sec. III. Then, the simplified models for the plasma plume expansion and interaction with the space debris are presented in Sec. IV. The independent optimization of the ITT is described and discussed in Sec. V. Sec. VI then presents the results of the overall propulsion subsystem optimization, including both the ITT and ICT. Finally, the conclusions of the study are reported in Sec. VII.

## II. Mission Specifications and Propulsion Subsystem Constraints

An IBS mission generally consists of two phases: a rendez-vous phase with the target debris object, out of the scope of this study, and a shepherding phase, in which the orbit change is carried out with the use of electric propulsion. The specifications of a realistic de-orbiting IBS mission are summarized in Tab. 1. A de-orbiting manoeuvre of approximately 300 km in 170 days, or equivalently a de-orbit rate of approx. 2 km/day, has been considered as the baseline mission goal. The debris object weighs 1.5 tons and currently orbits in a nearly-polar low Earth orbit. Considering an average 67% orbit daylight fraction (thrusters cannot operate on battery power alone, due to a S/C design choice), the above defined specifications on the debris mass and orbit decay rate are equivalent to constraining the transmitted force to the debris, $F_{TG}$, to 30 mN. Moreover, the operational distance between the ITT exhaust plane and the debris object must not be lower than 7 m. This threshold corresponds to the half span of the S/C solar array and has been chosen due to collision safety considerations in case of a failure of the relative attitude control. Finally, the IBS wet mass, $m_{IBS}$, is expected to be around 500 kg. The electric propulsion subsystem, which is in charge of transmitting the required force to the target, must comply with stringent power constraints at platform level. Referring to Tab. 2, the total input power to the power processing units (PPUs) of the EPS is limited to 3 kW. This means that, assuming a PPU energy conversion efficiency of 85% (a conservative value), this power limit corresponds to 2.6 kW at thruster level. Finally, regarding the power generation subsystem, a value of 13.3 kg/kW has been considered for the specific mass of

**Table 1 De-orbiting mission specifications and assumptions**

| Mission requirements and assumptions | Values | Units |
|---|---|---|
| IBS spacecraft mass, $m_{IBS}$ | 500 | kg |
| Target debris mass, $m_{TG}$ | $\simeq 1.5$ | tons |
| Target debris characteristic diameter | 2.5 | m |
| Orbit altitude change | 300 | km |
| Orbit altitude change per day | $\sim 2$ | km/day |
| Daylight fraction in orbit, $f_{light}$ | 67 | % |
| Shepherding phase duration, $\Delta t_{IBS}$ | 170 | days |
| Achieved target delta-V | 0.190 | km/s |
| Required force on the debris, $F_{TG}$ | 30 | mN |
| Operational distance, $d$, between ITT and target debris | $\geq 7$ | m |

**Table 2 IBS power constraints and assumptions**

| EPS constraints and assumptions | Values | Units |
|---|---|---|
| Input power to the EPS PPUs | $\leq 3$ | kW |
| PPUs efficiency, $\eta_{PPU}$ | 85 | % |
| Input power to both thrusters | $\leq 2.6$ | kW |
| Specific mass of the power generation subsystem, $\rho_{pwr}$ | 13.3 | kg/kW |

the dedicated solar arrays. This value is representative of the current available technology.

## III. Characterization of the ITT and ICT

In this study, both the ITT and the ICT are assumed to be radio-frequency ion thrusters. This is a particular type of gridded ion thruster, in which the ionization process is achieved through the inductively-coupled RF antenna, wrapped around the thruster chamber, as shown in Fig. 2. The generated ions are accelerated through a grid system to a kinetic energy given by $q_i \Delta\phi_B$, with $q_i$ representing the ion charge and $\Delta\phi_B$ the effective acceleration beam voltage. As shown in Fig. 2, this beam voltage is the effect of various contributions: the plasma voltage drop within the chamber (a few tens of Vs), $\Delta\phi_{chamber}$, the voltage drop between screen and acceleration grids (several kVs) and a final voltage increment, $\Delta\phi_{neut}$, that brings the potential to a value slightly higher than the

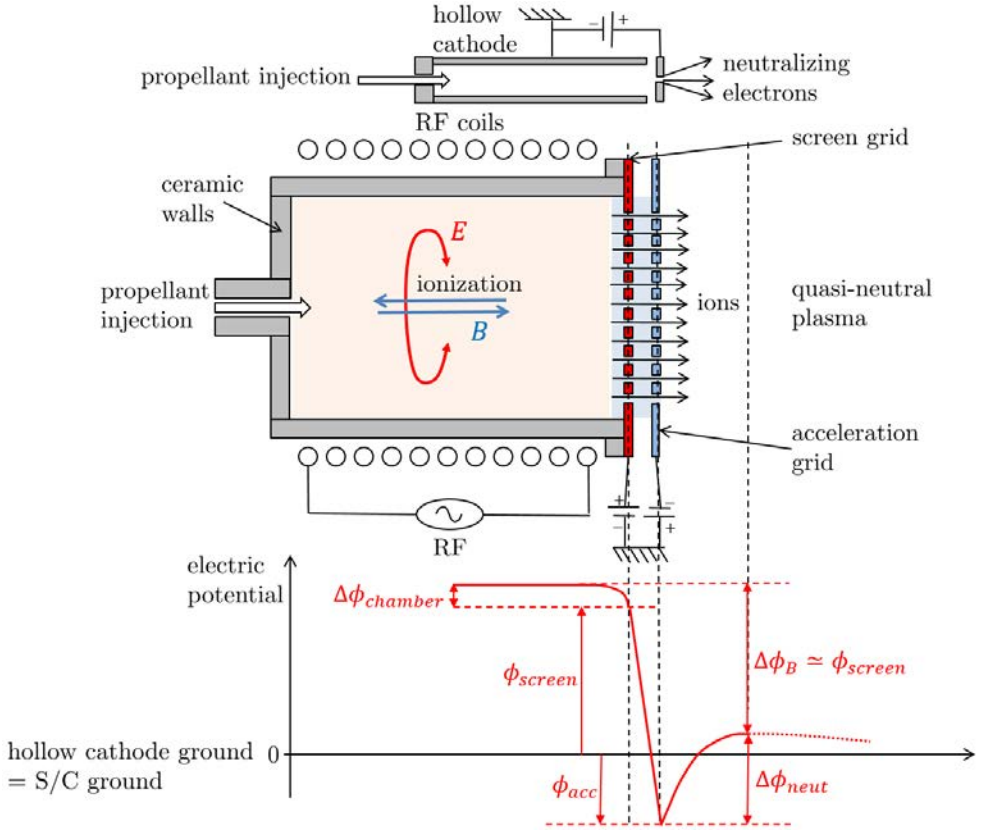


**Fig. 2 Generic working principle of a RIT thruster and electric potential evolution across the thruster symmetry axis. Voltage drops and lengths are not to scale**

potential of the neutralizing hollow cathode [12] (a few tens of Vs) and that is necessary to attract the neutralizing electrons. Since the hollow cathode is grounded, the effective beam acceleration voltage is well approximated by the screen grid potential:

$$\Delta\phi_B = \Delta\phi_{chamber} + (\phi_{screen} - \phi_{acc}) + \Delta\phi_{neut} \simeq \phi_{screen}. \tag{3}$$

For this optimization study, a thruster performance model is needed to explore the behavior of various thruster figures of merit as a function of some design parameters. The details and the justification of such a performance model can be found in Ref. [13]. Hereafter, only a summary of the main characteristics of the model is provided. Referring to Fig. 3, the required input variables (or design parameters) are the beam voltage, $\Delta\phi_B$, and the thrust force, $F$. The model then provides as output the thruster plume divergence angle, $\alpha_0$, the necessary beam current, $I_B$, the thruster radius, $R_{thr}$, the mass utilization efficiency, $\eta_m$, and the RF input power, $P_{RF}$, necessary to sustain

the discharge. These performance figures follow the dependencies shown in Eqs. 4 to 8:

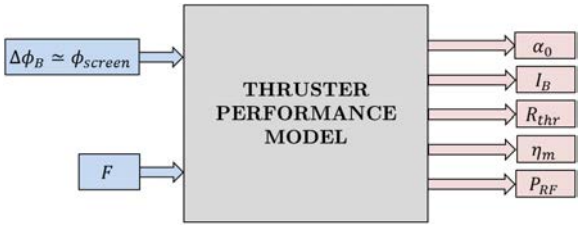


**Fig. 3 Block diagram of the performance model used for both the ITT and the ICT**

$$\alpha_0 \propto \Delta\phi_B^{-\beta_1} \tag{4}$$

$$I_B \propto F\Delta\phi_B^{-1/2} \tag{5}$$

$$R_{thr} \propto I_B^{1/2} \tag{6}$$

$$\eta_m \propto \ln(R_{thr}) \tag{7}$$

$$P_{RF} \propto R_{thr}^{\beta_2}. \tag{8}$$

First of all, the thruster divergence angle, $\alpha_0$, is modeled as a decreasing power law of the beam voltage, with a coefficient $\beta_1 > 1$, as shown in Eq. 4. The beam current is then proportional to the ratio between the thrust and the ion exhaust velocity (which scales as $\Delta\phi_B^{1/2}$), as shown in Eq. 5. Since the required ion extraction area is proportional to the beam current and grows with the square of the thruster radius, $R_{thr}$ is proportional to the square root of $I_B$, as dictated by Eq. 6. The mass utilization efficiency, $\eta_m$, increases logarithmically with the thruster radius according to Eq. 7, as a larger thruster requires a lower neutral gas pressure to sustain the RF discharge and hence features a lower neutral outflow fraction. The required RF input power is also modeled as a function of the thruster radius, and more precisely as a power law with coefficient $\beta_2 > 1$, so that a larger thruster requires a higher RF input power (Eq. 8).

With the performance figures computed above, it is then straightforward to obtain the beam power, $P_{beam}$, and hence the total thruster input power, $P = P_{beam} + P_{RF}$, the mass flow rate, $\dot{m}$, the specific impulse, $I_{sp}$, and the total thrust efficiency, $\eta_T$, following their classical definitions,

provided in Eqs. 9 to 13.

$$P_B = I_B \Delta\phi_B \tag{9}$$

$$P = P_{RF} + P_B \tag{10}$$

$$\dot{m} = \frac{m_i}{q_i}\frac{I_B}{\eta_m} \tag{11}$$

$$I_{sp} = \frac{F}{\dot{m} g_0} \tag{12}$$

$$\eta_T = \frac{F I_{sp}}{2P}. \tag{13}$$

The models for the ITT and for the ICT only differ in terms of the proportionality constants and power law coefficients in Eqs. 4 to 8, as discussed in Ref. [13].

## IV. Modeling the momentum transfer efficiency

### A. Simplified plume expansion and debris interaction models

A detailed description of the physical phenomena taking place in a plasma plume expansion into vacuum is provided in Refs. [8] and [9]. In summary, the plasma plume generated by a plasma thruster can be divided into two regions as sketched in Fig. 4. First, a near region extending up to a few thruster radii from the thruster exit where collisions, thruster electromagnetic fields and neutralizer 3D effects dominate the expansion, and where the ion beamlets coalesce into a single-peaked beam. Second, a far region plume, where these effects become negligible and the smooth, single-peaked profile continues to expand under the influence of the residual electron pressure and ambipolar electric field. The complex near-region plume cannot be easily modeled in terms of simple equations, and it is usually characterized experimentally. The far-region plume, on the other hand, can be studied with simplified fluid models, like those in Refs. [8, 9]. Referring to Fig. 4, we begin by defining a reference frame based on an initial plane located within the far region, at a distance $d_0$ from the thruster exit. Existing experimental observations of gridded ion thrusters and Hall effect thrusters show that the plume has already become smooth and single-peaked beyond one or two thruster radii from the thruster exit [14–16]. Following the self-similar plume solution (SSM) method, firstly introduced by Parks [17], at this initial plane, the plume is assumed to have a Gaussian density profile, a constant axial velocity and a linearly increasing radial velocity. Moreover,

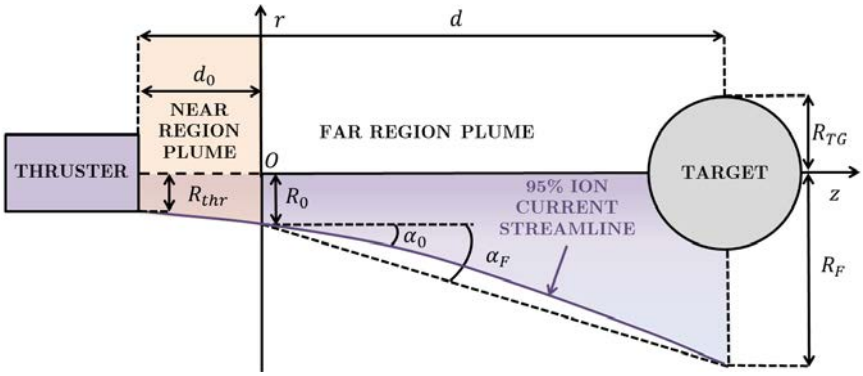


**Fig. 4 Sketch of the plasma plume near and far regions, the plasma streamtube containing 95% of the ion current, and the target debris**

the streamtube containing 95% of the ion current has a radius $R_0$ and a half-cone angle given by the thruster divergence angle, $\alpha_0$, as shown in Fig. 4.

Given the impossibility to obtain experimental near region data at this design stage of the project, we shall further assume that our far region starts at the exit plane of the thruster (i.e. we take $d_0 = 0$), where the ITT performance model provides the corresponding plume divergence angle, $\alpha_0$. To cover for the potential divergence increase in the near-region, a +10% margin on this initial divergence angle (or thruster divergence angle) has been included in the following analyses.

The SSM method then allows to compute the plasma density and velocity through a self-similar expansion function $h$, which obeys Eq. 14 and can be obtained through numerical integration with the initial condition $h(0) = 1$. In this differential equation, $\tilde{z} = z/R_0$ is the normalized axial coordinate and $M_0$ is the initial ion Mach number, whose square represents the ratio between the ion kinetic energy and the electron thermal energy, as shown in Eq. 15, where $m_i$ and $q_i$ are the ion mass and charge (we assume singly charged Xenon ions) and $T_{e0}$ is the electron temperature at the origin $O$ of the reference frame of Fig. 4:

$$\frac{dh}{d\tilde{z}} = \sqrt{\tan^2\alpha_0 + 12\frac{\ln h}{M_0^2}} \quad ; \quad h(0) = 1 \tag{14}$$

$$M_0 = \sqrt{\frac{m_i u_{i0}^2}{T_{e0}}} = \sqrt{\frac{2q_i\Delta\phi_B}{T_{e0}}}. \tag{15}$$

The 95% ion current streamtube radius, $R(z)$, the axial and radial plume velocity, $u_z(r,z)$ and $u_r(r,z)$, and the plume density, $n(r,z)$, are finally obtained with Eqs. 16 to 19. Here $n_0$ and $u_{i0}$

represent the plasma density and ion velocity at the origin $O$:

$$R(z) = R_0 h(\tilde{z}) \tag{16}$$

$$u_z(r,z) = u_{i0} \tag{17}$$

$$u_r(r,z) = u_{i0} \frac{dh}{d\tilde{z}}(\tilde{z}) \frac{r}{R(z)} \tag{18}$$

$$n(r,z) = \frac{n_0}{h^2(\tilde{z})} \exp\left(-3\frac{r^2}{R^2(z)}\right). \tag{19}$$

It is worth to mention that the self-similar solution of Eq. 14 and Eqs. 16 to 19 is valid only for isothermal electrons. Other thermodynamic models for the electrons can be easily employed, such as polytropic electrons, however, the isothermal limit is conservative, in the sense that it causes the largest increase of plume divergence and hence, in the context of an IBS mission, the lowest momentum transfer efficiency [8, 9]. The electron temperature appearing in Eq. 14 (through $M_0$) assumes values around 2-3 eV [14, 15] in Hall Effect thrusters and between 1 and 3 eV in ion thrusters [16]. Therefore, we have assumed the conservative value of $T_{e0} = 3$ eV, as shown in Tab. 3. In fact, the higher the electron temperature and their thermal energy, the higher the increase of divergence in the plume. On the contrary, if we progressively decrease the electron temperature to 0, we get the limit of $M_0 \to \infty$, for which the self similar function can be easily solved as $h(\tilde{z}) = 1 + \tilde{z}\tan\alpha_0$, corresponding to a perfectly conical plume expansion.

With the plume solution of Eq. 14 and Eqs. 16 to 19, and following the approach of Ref. [10], a simplified formula for the fraction of plume momentum intercepted by the debris can be obtained. Firstly, to simplify the analysis, the debris is modelled as an equivalent sphere of radius $R_{TG} = 1.25$ m (half of the characteristic diameter of the target debris, given in Tab. 1) and its center is located at a distance $d$ from the thruster exit plane. At this distance, assumed equal to 7 m (the minimum operational distance of Tab. 1), the radius of the plasma tube carrying 95% of the ion current is $R_F$, which allows us to define an equivalent conical divergence angle at the debris, $\alpha_F$, as:

$$\alpha_F = \arctan\left(\frac{R_F - R_0}{d}\right) > \alpha_0. \tag{20}$$

Note that $\alpha_F$ is *not* the local slope angle of the 95% ion current streamline, as clearly shown in Fig. 4. Integrating the plasma momentum over the surface of the sphere, we can finally compute

the momentum transfer efficiency as:

$$\eta_B = 1 - \exp\left(-\frac{3 \cdot R_{TG}^2}{R_F^2 - (\tan\alpha_F \cdot R_{TG})^2}\right). \tag{21}$$

The assumptions described so far for the characterization of the momentum transfer efficiency are finally summarized in Tab. 3.

**Table 3 Parameters affecting the plume expansion and target interaction**

| Plume and debris interaction parameters | Values | Units |
|---|---|---|
| Electron temperature, $T_{e0}$, at the origin O | 3.0 | eV |
| Equivalent spherical radius, $R_{TG}$, of the debris | 1.25 | m |
| Near region axial length, $d_0$ | 0.0 | m |
| Distance between thruster exit and debris centre, $d$ | 7.0 | m |
| Margin on $\alpha_0$ to account for near region effects | 10.0 | % |
| Propellant ions type | n/a | Xenon |
| Ions charge, $q_i$ | $1.6 \cdot 10^{-19}$ | C |

### B. Equivalent conical divergence angle at the debris and momentum transfer efficiency

In this section, the effect of the ITT beam voltage on $\alpha_F$ and $\eta_B$ is assessed and discussed. With the use of the plume model described in Sec. IV A and with the parameters of Tab. 3, we can obtain a 2-D map of the equivalent conical divergence angle and of the momentum transfer efficiency as a function of $\Delta\phi_B$ and $\alpha_0$ for 2 different values of $R_0$ (7 and 25 cm), whose range should include the design radius of the ITT thruster.

Referring to Fig. 5 (a), as the beam voltage, $\Delta\phi_B$, or the initial divergence angle, $\alpha_0$, increase, the difference between the near and equivalent conical divergence angles becomes smaller. Asymptotically, $\alpha_F$ tends to $\alpha_0$ for both increasing beam voltage and near region divergence angle. Regarding the initial plume radius effect, the higher plume radius yields a lower equivalent divergence angle at the debris, because the radial electron pressure gradients at the initial plume plane are lower, thus yielding a lower divergence increase.

Fig. 5 (b) shows the corresponding dependence of the momentum transfer efficiency on $\Delta\phi_B$ and $\alpha_0$ for the two initial radius cases. The momentum transfer efficiency increases substantially for

decreasing divergence angles, and, for a given $\alpha_0$, it shows a weak dependence on the beam voltage, except at very low voltage and small initial divergence angle. The effect of the initial plume radius, on the other hand, is twofold. At a sufficiently high beam voltage or divergence angle, when the electron pressure effects are negligible, a higher initial plume radius $R_0$ yields automatically a higher radius $R_F$ at the target debris and hence a lower momentum transfer efficiency (through Eq. 21). At small initial divergence angles and beam voltages, on the other hand, the increase in divergence angle plays a more important role than the initial plume radius, so that a lower initial radius also yields a lower momentum transfer efficiency.

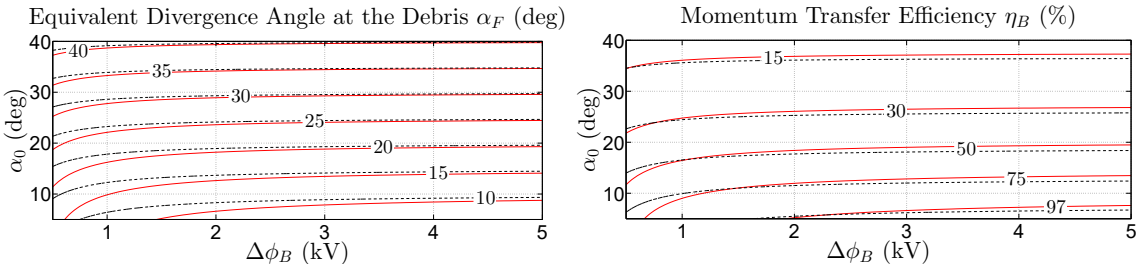


(a) (b)

**Fig. 5 (a) Equivalent conical divergence angle at 7 m as a function of the beam voltage, $\Delta\phi_B$, and initial divergence angle, $\alpha_0$, for $R_0$ = 7 cm (red solid lines) and 25 cm (black dashed lines). (b) Momentum transfer efficiency as a function of the beam voltage, $\Delta\phi_B$, and initial divergence angle, $\alpha_0$, for $R_0$ = 7 cm (red solid lines) and 25 cm (black dashed lines).**

In our ITT performance model, the near region divergence angle, $\alpha_0$, is a direct function of the beam voltage, as given by Eq. 4, so that the momentum transfer efficiency (and the equivalent conical divergence angle at the debris) is indeed a function of $\Delta\phi_B$ and $R_0$.

In order to evaluate the real effect of the initial plume radius $R_0$ on the momentum transfer efficiency for our ITT, $\eta_B$ has been evaluated again for the two different initial radius cases (7 and 25 cm). The use of the thruster performance model of Sec. III has been limited to Eq. 4 to model the dependence of the initial divergence angle on $\Delta\phi_B$ (Eq. 6 has not been considered here). The momentum transfer efficiency evolution with $\Delta\phi_B$ is shown in Fig. 6. At low beam voltages (below 2.5 kV), the momentum transfer efficiency increases almost linearly with $\Delta\phi_B$, while at higher voltages (above 2.5 kV) the increase becomes weaker, saturating at almost 100% for voltages above 4.5 kV.

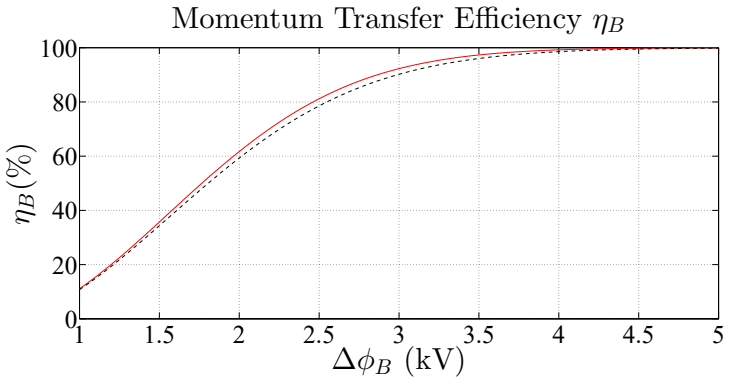


**Fig. 6 Momentum transfer efficiency, $\eta_B$, as a function of the ITT beam voltage, $\Delta\phi_B$, for two initial plume radii: 7cm (red solid line) and 25 cm (black dashed line). Eq. 4 has been used to obtain $\alpha_0$ as a function of $\Delta\phi_B$**

Although the differences between the two $R_0$ cases are small (always lower than 5%), the worst case scenario is clearly represented by the higher initial radius case (25 cm). The 25 cm case has then been considered to model conservatively the dependence of $\eta_B$ on $\Delta\phi_B$ in the optimization study described in the following sections.

Before proceeding with it, however, it is worth to further discuss the plume expansion effects on the momentum transfer efficiency. Referring to Fig. 5 (a), it is apparent that the more hypersonic (the higher $M_0$ or $\Delta\phi_B$) and the more divergent (the higher $\alpha_0$) the plume is, the closer to conical its expansion. This conical-like expansion is the major source of momentum transfer efficiency loss, as shown in Fig. 5 (b), where the iso-$\eta_B$ lines are almost horizontal and showing a weak dependence on the beam voltage. Under a purely "geometrical" expansion the plume density decreases with the square of its streamline radius, which is proportional to both the operational distance and $\tan(\alpha_0)$. Therefore, it is paramount to minimize $\alpha_0$, which generally requires operating at a high beam voltage (Fig. 6).

Secondly, even if the initial divergence angle is small, the residual electron pressure makes the plume expand further, meaning that the slope of the ion streamlines increases away from the thruster [8, 9]. This effect is small in our case, except at very low $\Delta\phi_B$ and $\alpha_0$ (where the iso-$\eta_B$ and iso-$\alpha_F$ lines of Fig. 5 (a) and (b) deviate from horizontal lines), and can always be mitigated by increasing the operating Mach number, $M_0$, provided by Eq. 15. For a fixed propellant atom mass, this can be

achieved by either increasing the beam voltage, $\Delta\phi_B$, or reducing the residual electron temperature, $T_{e0}$, in the plume.

## V. Optimization of the ITT

Before proceeding with the optimization of the overall EPS, it is useful to firstly optimize the ITT independently. This means to identify the operating beam voltage of the ITT that maximizes some specific figure of merit. As explained in Ref. [13], a key figure of merit for the ITT is the ratio between transmitted force to the debris and input power to the thruster. Referring to Fig. 6, if we operate at a constant ITT thrust, the transferred thrust to the debris grows linearly with $\Delta\phi_B$ at low beam voltages (Fig. 6), while the required input power grows with $\Delta\phi_B^{1/2}$ (Eqs. 9 and 5 with $F$ constant). The transferred thrust to power ratio thus increases with $\Delta\phi_B$ until the momentum transfer efficiency begins to saturate and its increase is equal to the increase in input power. The voltage corresponding to this maximum transferred thrust to power ratio represents the optimal ITT operational condition.

A method to maximize the above defined figure of merit is described hereafter. By fixing the transmitted force on the target to the required 30 mN value (see Tab. 1), we shall look for the operational voltage that minimizes the required ITT input power. First, we compute the required ITT thrust as a function of $\Delta\phi_B$, with the conservative curve of Fig. 6 to express the momentum transfer efficiency:

$$F_{ITT}(\Delta\phi_B) = \frac{30 \text{ mN}}{\eta_B(\Delta\phi_B)}. \tag{22}$$

Then, once $\Delta\phi_B$ and $F_{ITT}$ are fixed, with the use of the performance model of Sec. III, all the thruster performance figures can be obtained, including the input thruster power, $P_{ITT}$. This power is finally plotted in Fig. 7 as a function of $\Delta\phi_B$. As expected a minimum operating power is found at a $\Delta\phi_B = 3.3$ kV, with a corresponding thrust force of 31.9 mN and a momentum transfer efficiency of 94.1 %.

The choice of the design voltage of the ITT, however, cannot be determined solely by the maximization of the transferred force to power ratio. A key figure of merit of the ITT is, in fact, the mass utilization efficiency, $\eta_m$, which should be high. In fact, a low $\eta_m$ can cause a high number of

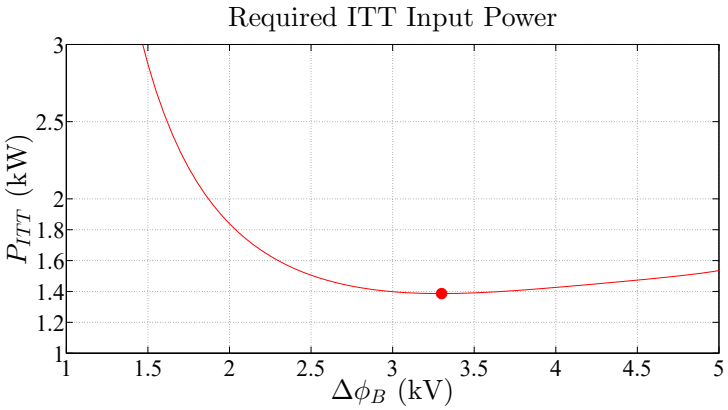


**Fig. 7 ITT input power required to transfer a force of 30 mN to the target debris, with the mission specifications and plume parameters of Tab. 1 and Tab. 3. The optimal operations point is shown with a red dot**

charge-exchange collisions between ions and neutrals atoms in the near region, and hence a large ion backflow towards sensitive S/C surfaces, which could potentially endanger the mission, or increase the initial plume divergence, $\alpha_0$, beyond the values assumed here.

At the optimal ITT point discussed above, the mass utilization efficiency turns out to be 72.2% (according to the ITT performance model). Although it is out of the scope of this paper to assess the effects of such efficiency, it is a key aspect to model when designing a real mission.

## VI. Optimization of the whole electric propulsion subsystem

### A. Major assumptions

The optimization described in Sec. V provides very valuable inputs for the choice of the operational point of the ITT alone. Nevertheless, from an overall subsystem perspective, what needs to be minimized are the input power to the two thrusters, $P^*$, and the fraction of the EPS dedicated mass that can be optimized, $m^*$. In this section, we shall describe the approach we have followed to define the optimal operational points (or beam voltages) of the two thrusters that minimize $P^*$ and $m^*$.

The total thruster input power to be optimized, $P^*$, is simply given by:

$$P^* = P_{ITT} + P_{ICT}, \tag{23}$$

while the definition of $m^*$ is less straightforward. The total EPS dedicated mass can be split into

several contributions: the two thrusters mass, $m_{ITT} + m_{ICT}$, the total dedicated power generation subsystem mass, $m_{pwr}$ (solar arrays fraction dedicated to the generation of the PPUs input power), the total propellant mass, $m_{prop}$, and the power processing units mass, $m_{PPU}$. In this study, however, we have considered for $m^*$ only a part of the above defined EPS dedicated mass, as shown in Eq. 24:

$$m^* = m_{pwr} + m_{prop}. \tag{24}$$

In fact, the mass contributions of the thrusters and of the PPUs have not been included, as their variations with the operational beam voltage is expected to be quite small. The former (thruster units masses) would slightly depend on the operating conditions, as a higher voltage yields a lower mass flow rate and hence a smaller and lighter thruster [13]. However, a thruster unit weighs only a few kg (at these power levels) and hence, its mass variation can be neglected with respect to the major mass contributions: $m_{pwr}$ and $m_{prop}$. Regarding the PPUs, on the other hand, their mass can hardly be modelled as a linear function of $\Delta\phi_B$ and their mass variation is expected to be small (in the considered range of beam voltages). The remaining mass contributions are modeled as given by Eqs. 25 and 26:

$$m_{prop} = f_{light}\Delta t_{IBS}\left(\dot{m}_{ITT} + \dot{m}_{ICT}\right) \tag{25}$$

$$m_{pwr} = \frac{\rho_{pwr}P^*}{\eta_{PPU}}, \tag{26}$$

where $f_{light}$ and $\Delta t_{IBS}$ are respectively the orbital period fraction in daylight conditions and the shepherding phase duration, $\dot{m}_{ITT}$ and $\dot{m}_{ICT}$ are the mass flow rates of the ITT and ICT, and $\rho_{pwr}$, $\eta_{PPU}$ are respectively the solar array specific mass and the PPUs energy conversion efficiency.

Finally, the values of all the parameters required by the EPS optimization study are listed in Tabs. 1 and 2.

### B. Overall Optimization Method

The electric propulsion subsystem optimization consists in studying the evolution of figures of merit such as the total thruster input power, $P^*$, the optimizable EPS mass, $m^*$, the total required propellant mass, $m_{prop}$, and the equivalent shepherding delta-V, $\Delta V_{eq}$, as 2-D functions of $\Delta\phi_{B,ITT}$

and $\Delta\phi_{B,ICT}$. For any ITT beam voltage, $\Delta\phi_{B,ITT}$:

1. The ITT thruster parameters are computed following the approach of Sec. V with the model of Ref. [13] (described in Sec. III)

2. Given the ITT thrust, $F_{ITT}$, the required ICT thrust is obtained through Eq. 2

3. For a varying ICT beam voltage in a range between 0.5 and 5 kV, the following parameters are computed:

   - The ICT thruster performance figures, with the model of Ref. [13] (described in Sec. III)
   - The overall (ITT+ICT) thruster input power, $P^* = P_{ICT} + P_{ITT}$
   - The overall required propellant mass, $m_{prop}$, using Eq. 25
   - The overall power subsystem dedicated mass, $m_{pwr}$, using Eq. 26
   - The equivalent shepherding phase delta-V, $\Delta V_{eq}$. An equivalent propulsion subsystem specific impulse is first obtained as:

$$I_{sp,eq} = \frac{(\dot{m}_{ITT} I_{sp,ITT} + \dot{m}_{ICT} I_{sp,ICT})}{(\dot{m}_{ITT} + \dot{m}_{ICT})} \tag{27}$$

     where $I_{sp,ITT}$ and $I_{sp,ICT}$ are respectively the ITT and ICT specific impulses. Then, through Tsiolkovsky's equation, $\Delta V_{eq}$ is computed as:

$$\Delta V_{eq} = I_{sp,eq} g_0 \ln\left(\frac{m_{IBS}}{m_{IBS} - m_{prop}}\right) \tag{28}$$

     where $g_0$ is the standard gravity acceleration constant.

### C. Overall Optimization Results

Following the procedure described in the previous paragraph, the 2-D contours of Fig. 8 have been obtained. Fig. 8 (a) shows the total thruster input power, $P^*$. For a given ITT voltage, the total power presents a minimum at an ICT voltage of approx. 1000 V. Then, it starts to increase again because, for a given ICT thrust, the required ICT power grows with the ICT specific impulse (or beam voltage). The lowest total power is 2.54 kW, achieved at the ITT-ICT voltages point (3.58, 1.01) kV. At this point, $F_{ITT} = 31.1$ mN and $F_{ICT} = 40.6$ mN. It is important to underline that

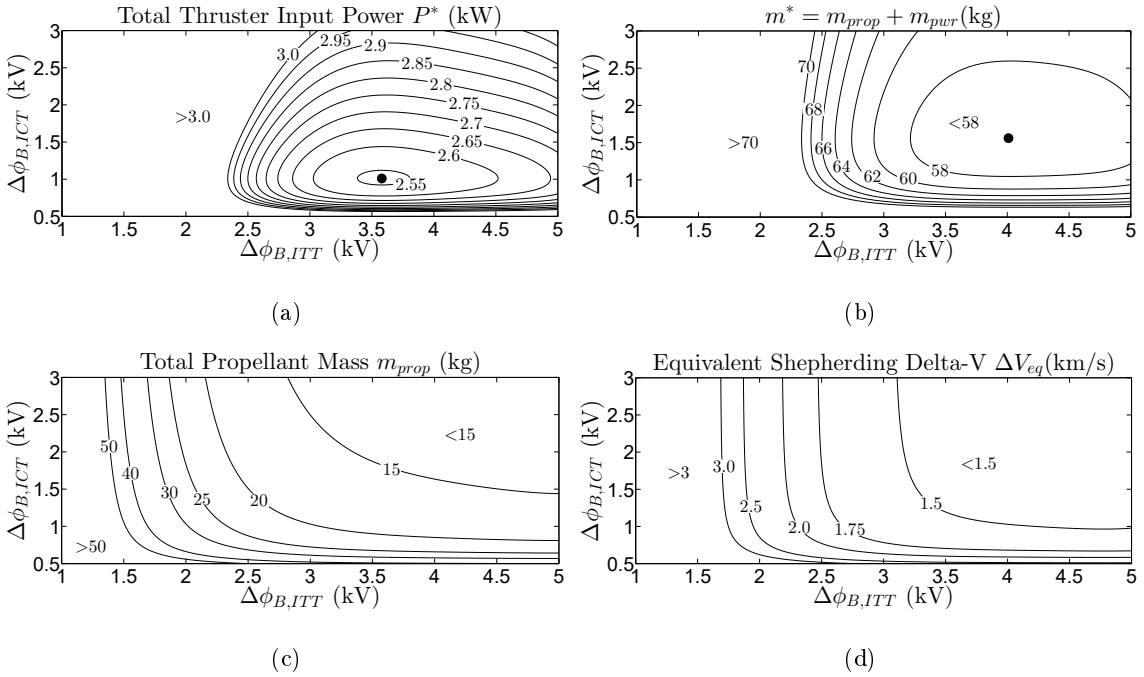


**Fig. 8 (a) Total input power to the thrusters, $P^* = P_{ITT} + P_{ICT}$, with the corresponding minimum shown with a black dot. (b) Optimizable EPS dedicated mass, $m^* = m_{prop} + m_{pwr}$, with the corresponding minimum shown with a black dot. (c) Total propellant mass of the shepherding phase, $m_{prop}$. (d) Equivalent shepherding phase delta-V, $\Delta V_{eq}$.**

small changes in the ITT voltage around this optimal point produce no significant variation in the total thruster power.

Fig. 8 (b) shows the optimizable EPS dedicated mass, $m^*$. The optimal point now shifts to higher voltages for both the ITT and the ICT with respect to that of Fig. 8 (a), because the total propellant mass decreases for increasing voltages. The optimal voltages (corresponding to a total mass of 56.6 kg) are (4.01, 1.56) kV. At this point, $F_{ITT} = 30.5$ mN and $F_{ICT} = 40.1$ mN. Observe that, for a wide region around the optimal point, variations in both the ITT and ICT voltage produce no significant changes in $m^*$. Moreover, the total mass savings that an optimized design yields are quite small (10-15 kg), when compared to the total expected IBS mass (500 kg).

Fig. 8 (c) shows the total propellant mass of the shepherding phase as a function of both the ITT and the ICT beam voltages. Clearly, the higher these voltages, the lower the overall propellant mass. However, the propellant mass savings of an optimized design are, again, quite small. For example, at $\Delta\phi_B = 3.5$ kV, increasing the ICT voltage from 1 to 2 kV only yields a mass saving of

5 kg.

Finally, Fig. 8 (d) shows the equivalent shepherding delta-V, $\Delta V_{eq}$. As expected, for an ICT voltage above 1-1.5 kV, the delta-V depends essentially on the momentum transfer efficiency and hence on the ITT voltage alone: the higher the ITT voltage, the lower the $\Delta V_{eq}$. At low ICT voltages however, the divergence losses of the ICT become important and this means that the ICT mass flow necessary to achieve the required thrust increases as the voltage decreases. For this reason, the equivalent shepherding delta-V increases substantially as the ICT voltage becomes smaller. It is also pointed out that $\Delta V_{eq}$ does not represent the inertial velocity change of either the target or the IBS (shown in Tab. 1), but rather the propulsion delta-V of a thruster, which is equivalent (in terms of mass consumption) to the ITT-ICT system.

The main conclusion that can be extracted from the presented results is that the optimal points for the ICT and ITT beam voltage are very different. The need to guarantee a sufficiently high momentum transfer efficiency drives the optimal ITT voltage to higher values. For the ICT, on the other hand, as long as the thruster efficiency is not strongly affected, a lower voltage allows to keep the required power low, at the expense of a higher propellant consumption. This results into an ICT optimal beam voltage, which is generally quite lower than that of the ITT.

The optimal design choice may be either based on the total dedicated mass or on the total thruster power, depending on the specific mission constraints. For example, for missions featuring a well defined limit for the total platform power, minimization of the total thruster power should be pursued (Fig. 8 (a)). For other missions not featuring such a stringent constraint, the total dedicated mass would represent a more adequate figure of merit for the overall electric propulsion subsystem (Fig. 8 (b)). Nonetheless, as seen in this analysis for a single de-orbiting mission, $m^*$ is quite small with respect to the total IBS wet mass (10%), and therefore the dedicated mass optimization has only a small impact on the total mass budget.

## VII. Conclusions

This paper has presented a dedicated study of the optimization of the electric propulsion subsystem of an ion beam shepherd mission, a novel technique for contactless debris de-orbiting/relocation

that requires two electric thrusters: an impulse transfer thruster and an impulse compensation thruster. The optimal operational points of the ITT alone and of the two thrusters considered simultaneously, expressed in terms of their beam voltages, have been identified and the corresponding optimization method described.

Dedicated design performance models [13] have been used to model the effects of changes in the operational conditions of both thrusters (beam voltage and thrust) on their performance figures.

Then, simplified plasma plume and target interaction models have been used to characterize numerically the momentum transfer efficiency, and it has been found that, for the given mission scenario, the plume physics clearly affects the design choice. First of all, the thruster must guarantee a small initial divergence angle, as the conical beam expansion is the major factor that reduces the momentum transfer to the target and hence the efficiency of the IBS technique. Secondly, a high operational voltage also reduces the increase of the beam divergence due to electron thermal effects.

From the point of view of the ITT alone, it is found that an optimal beam voltage exists that maximizes the transmitted force to power ratio, or equivalently that minimizes the required power for a given force on the target.

The optimization study for the whole electric propulsion subsystem has permitted to identify the optimal operational points of both thrusters simultaneously, finding that the minimum total dedicated mass or power are minimized for two different beam voltages of ITT and ICT, being that of the ITT much higher. The choice on whether to minimize the total dedicated mass or the total thruster power depends on the individual mission specifications.

The study presented in this paper can be further refined in the future, by introducing additional effects in the total EPS mass budget, such as the influence of the mass of the thruster units and of the dedicated PPUs. Finally, although both thrusters have been considered of the same type (radio-frequency ion thrusters) to reduce the system complexity, using a different technology for the ICT (e.g. a Hall effect thruster) is also envisaged and should be further investigated.

**Acknowledgments**

The research leading to the results of this paper has been carried out within the *LEOSWEEP* project ("Improving Low Earth Orbit Security With Enhanced Electric Propulsion") and has received funding from the European Union Seventh Framework Programme (FP7/2007-2013) under grant agreement N.607457. Additional funding has been received by Spain's R&D National Plan, grant ESP2013-41052

**References**

[1] J.C. Liou and N.L. Johnson. A sensitivity study of the effectiveness of active debris removal in leo. *Acta Astronautica*, 64(2-3):236–243, 2009.

[2] J.C. Liou, N.L. Johnson, and N.M. Hill. Controlling the growth of future leo debris populations with active debris removal. *Acta Astronautica*, 66:648–653, 2010.

[3] L. Jasper, P. Andersony, H. Schaubz, and D. McKnight. Economic and risk challenges of operating in the current space debris environment. In *3rd European Workshop on Space Debris Modeling and Remediation*, CNES, Paris, 2014.

[4] C. Bombardelli and J. Peláez. Ion beam shepherd for contactless space debris removal. *Journal of Guidance, Control, and Dynamics*, 34(3):916–920, May 2011.

[5] C. Bombardelli, H. Urrutxua, M. Merino, E. Ahedo, and J. Peláez. The ion beam shepherd: A new concept for asteroid deflection. *AA*, 90(1):98 – 102, 2013.

[6] M. Merino, E. Ahedo, C. Bombardelli, H. Urrutxua, and J. Peláez. Ion beam shepherd satellite for space debris removal. In Luigi T. DeLuca, Christophe Bonnal, Oskar J. Haidn, and Sergey M. Frolov, editors, *Progress in Propulsion Physics*, volume IV of *EUCASS Advances in Aerospace Sciences*, chapter 8, pages 789–802. Torus Press, 2013.

[7] M. Ruiz, I. Urdampilleta, C. Bombardelli, E. Ahedo, M. Merino, and F. Cichocki. The FP7 LEOSWEEP project: Improving low earth orbit security with enhanced electric propulsion. In *Space Propulsion 2014*, Cologne, France, 2014.

[8] F. Cichocki, Merino M., and Ahedo E. Modeling and simulation of ep plasma plume expansion into vacuum. In *50th AIAA/ASME/SAE/ASEE Joint Propulsion Conference, Cleveland, OH*, AIAA 2014-3828, 2014.

[9] M. Merino, F. Cichocki, and E. Ahedo. Collisionless plasma thruster plume expansion model. *Plasma Sources Science and Technology*, 24(3):035006, 2015.

[10] C. Bombardelli, H. Urrutxua, M. Merino, E. Ahedo, and J. Peláez. Relative dynamics and control of an ion beam shepherd satellite. In James V. McAdams, David P. McKinley, Matthew M. Berry, and Keith L. Jenkins, editors, *Spaceflight mechanics 2012*, volume 143 of *Advances in the Astronautical Sciences*, pages 2145–2158. Univelt, 2012.

[11] F. Cichocki, M. Merino, E. Ahedo, D. Feili, and M. Ruiz. Electric propulsion subsystem optimization for ion beam shepherd missions. In *34th International Electric Propulsion Conference and 6th Nano-satellite Symposium, Hyogo-Kobe, Japan*, IEPC-2015-IEPC-35, 2015.

[12] Dan M. Goebel and Ira Katz. *Fundamentals of Electric Propulsion: Ion and Hall Thrusters*. JPL, 2008.

[13] D. Feili, M. Ruiz, M. Merino, F. Cichocki, E. Ahedo, M. Smirnova, and M. Dobkevicius. Impulse transfer thruster for an ion beam shepherd mission. In *34th International Electric Propulsion Conference*, IEPC-382, 2015.

[14] B.E. Beal, A. Gallimore, and J.M. Haas W.A. Hargus. Plasma properties in the plume of a hall thruster cluster. *Journal of Propulsion and Power*, 20(20):985 – 991, 2004.

[15] I.D. Boyd and J.T. Yim. Modeling of the near field plume of a Hall thruster. *Journal of applied physics*, 95:4575, 2004.

[16] J.E. Foster, G.C. Soulas, and M.J. Patterson. Plume and discharge plasma measurements of an nstar-type ion thruster. In *36th Joint Propulsion Conference and Exhibit, Huntsville, Alabama*, 2000.

[17] D.E. Parks and I. Katz. A preliminary model of ion beam neutralization. In *14th International Electric Propulsion Conference*, Fairview Park, OH, 1979. Electric Rocket Propulsion Society.